

**A novel critical distance-based homogenised material approach to estimate fatigue lifetime of plain/notched polylactide 3D-printed with different in-fill levels**

YAREN, Mehmet F <<http://orcid.org/0000-0002-7739-0794>> and SUSMEL, Luca <<http://orcid.org/0000-0001-7753-9176>>

Available from Sheffield Hallam University Research Archive (SHURA) at:

<https://shura.shu.ac.uk/35155/>

---

This document is the Published Version [VoR]

**Citation:**

YAREN, Mehmet F and SUSMEL, Luca (2025). A novel critical distance-based homogenised material approach to estimate fatigue lifetime of plain/notched polylactide 3D-printed with different in-fill levels. *International Journal of Fatigue*, 193: 108750. [Article]

---

**Copyright and re-use policy**

See <http://shura.shu.ac.uk/information.html>



# A novel critical distance-based homogenised material approach to estimate fatigue lifetime of plain/notched polylactide 3D-printed with different in-fill levels

Mehmet F. Yaren<sup>a</sup>, Luca Susmel<sup>b,\*</sup>

<sup>a</sup> Department of Mechanical Engineering, Sakarya University, 54050, Sakarya, Turkey

<sup>b</sup> Materials and Engineering Research Institute (MERI), Sheffield Hallam University, Harmer Building, Sheffield, S1 1WB, United Kingdom

## ARTICLE INFO

### Keywords:

Additive manufacturing  
polylactide (PLA)  
Voids  
Fatigue  
Critical distance  
Notch

## ABSTRACT

This study presents a novel approach to predict the fatigue life of plain and notched polylactide (PLA) components 3D-printed with different in-fill levels. The proposed method models 3D-printed PLA with manufacturing voids as a continuous, homogeneous, linear-elastic, isotropic material weakened by equivalent cracks that scale with the size of the voids. This allows for accurate estimation of both plain material strength and notched component fatigue life, considering various in-fill levels.

The proposed design method's accuracy and reliability were validated against extensive fatigue testing data from plain and notched specimens, fabricated with varying in-fill levels and raster angles. The strong correlation between predicted and experimental fatigue lives confirms that the method accurately assesses the fatigue strength of additively manufactured PLA components, even without explicitly modelling fabrication voids.

## 1. Introduction

Nowadays, Additive Manufacturing (AM) is used in a wide range of industries, including aerospace, biomedical, robotics, construction, and energy. The major advantage of the AM technology is its capability to produce complex geometries that are unfeasible or impossible to achieve with conventional methods. In this context, AM also allows for the manufacturing of objects with intricate internal structures, where the inner voids have controlled shapes, dimensions, and positions. This process can be optimized to obtain lighter structures that still fulfil their structural function. Additionally, internal voids can be used not only to reduce the weight of parts but also for various functional purposes. For instance, cooling channels [1], integrated sensors [2], and shapes suitable for negative Poisson's ratios (auxetic materials) [3] can be created by designing bespoke internal structures.

A wide range of materials can be used in AM, including ceramics, metals, and polymers. In AM various technologies are used, including stereolithography (SLA), selective laser sintering (SLS), direct energy deposition (DED) and fused deposition modelling (FDM). Among this wide variety of materials, polylactic acid (PLA) is one of the most popular due to its affordability and ease of manufacturing. PLA is a thermoplastic polymer, meaning it softens and becomes malleable when

heated and solidifies upon cooling. This makes PLA particularly suitable for 3D printing applications with FDM. PLA is a biodegradable polymer originally made from renewable plant sources such as sugarcane or corn starch, and it breaks down through natural biological processes. These properties make PLA advantageous for medical applications. In health-care, additive manufacturing enables the creation of personalised solutions such as stents [4], custom implants and prosthetics [5]. Research on PLA-based porous scaffolds is noteworthy due to the material's biodegradability. Additionally, the use of 3D-printing to create porous structures allows for customised solutions for patients, which enhances treatment effectiveness and improves success rates [6,7].

Studies indicate that AM parameters significantly affect the mechanical properties of 3D-printed PLA [8,9,10]. Gomez-Gras et al. [11] investigated the effect of different manufacturing parameters on the rotating bending fatigue behaviour of PLA and found that honeycomb patterns performs better than the rectilinear patterns. They also observed that fatigue life increases by increasing the nozzle diameter, and layer height.

Regarding the effect of the raw material on the mechanical strength, pigments are seen to affect markedly the mechanical behaviour, and the highest strength is seen to be obtained with white filaments [8,12].

In their study on the effect of manufacturing parameters on the static and fatigue behaviour of bone scaffold parts, Bakhtiari et al. [7] showed

\* Corresponding author at: Materials and Engineering Research Institute (MERI), Sheffield Hallam University, Harmer Building, Sheffield, S1 1WB, UK.  
E-mail address: [l.susmel@shu.ac.uk](mailto:l.susmel@shu.ac.uk) (L. Susmel).

Nomenclature	
a	semi-crack length
a <sub>eq</sub>	equivalent semi-crack length
d <sub>v</sub>	effective size of manufacturing voids
f(d <sub>v</sub> )	transformation function
k	negative inverse slope of the plain fatigue curve
k <sub>n</sub>	negative inverse slope of the notch fatigue curve
k <sub>t</sub>	dimensionless transformation constant
r <sub>n</sub>	notch root radius
A, B	constants in the L <sub>M</sub> vs. N <sub>f</sub> power law
F <sub>max</sub>	maximum force in the cycle
L	critical distance in the high-cycle fatigue regime
L <sub>M</sub>	critical distance in the medium-cycle fatigue regime
N <sub>f</sub>	number of cycles to failure
N <sub>Ref</sub>	reference number of cycles to failure (N <sub>Ref</sub> = 2·10 <sup>6</sup> cycles to failure)
Oxyz	local system of coordinates
P <sub>S</sub>	probability of survival
R	load ratio (R=σ <sub>min</sub> /σ <sub>max</sub> )
T <sub>σ</sub>	scatter ratio of the endurance limit for 90 % and 10 % probabilities of survival
θ, r	polar system of coordinates
θ <sub>p</sub>	manufacturing angle
σ <sub>max</sub>	maximum value of the stress in the cycle
σ <sub>max,0</sub>	maximum value of the plain endurance limit at N <sub>Ref</sub> cycle to failure
σ <sub>max,0-50%</sub>	maximum value of the plain endurance limit at N <sub>Ref</sub> cycle to failure for P <sub>S</sub> = 50 %
σ <sub>n,max</sub>	maximum value of the nominal stress in the cycle
σ <sub>n,max,0-50%</sub>	maximum value of the nominal notch endurance limit at N <sub>Ref</sub> cycle to failure for P <sub>S</sub> = 50 %
ΔK <sub>th</sub>	threshold value of the stress intensity factor range
Δσ <sub>0</sub>	range of the plain fatigue limit
Δσ <sub>0, 50%</sub>	range of the plain fatigue limit for P <sub>S</sub> equal to 50 %
Δσ <sub>0n</sub>	range of the notch fatigue limit
Δσ <sub>0n, 50%</sub>	range of the notch fatigue limit for P <sub>S</sub> equal to 50 %
Δσ <sub>eff</sub>	range of the effective stress
Δσ <sub>0n</sub>	range of the nominal stress
Δσ <sub>y</sub>	range of the stress parallel to the y-axis

that the compressive strength of PLA porous structures is directly proportional to the extrusion thickness and inversely proportional to the nozzle temperature. In the same study, the +45/-45° manufacturing angle exhibited the best fatigue performance among specimens produced at different angles [7]. However, Ezech and Susmel's experimental work [13] demonstrated that the manufacturing angle has, from an engineering design point of view, a negligible effect on fatigue life as long as objects are printed flat on the build plate. Additional studies also indicate that increasing the in-fill level improves the fatigue behaviour of structures [7,11,14].

As far as AM PLA parts are concerned, Ahmed and Susmel [15] developed and validated an approach suitable for estimating the static strength of notched components manufactured with different in-fill levels. This design approach uses the equivalent homogenised cracked material concept and the Theory of Critical Distances (TCD). Owing to the remarkable accuracy shown by this approach, in this paper the above design method is reformulated to make it suitable for determining the medium-cycle fatigue strength of PLA additively manufactured by adopting different in-fill levels. The following sections will cover the theoretical background, specimen manufacturing, test setup, fatigue results, and model verification.

## 2. The TCD to estimate fatigue strength

Geometrical features, often referred to as “notches”, have always been a major concern for structural engineers due to their detrimental effect on the overall static and fatigue behaviour of real structural components. Various methods have been proposed for static and fatigue assessment of notched materials. For notched metals under fatigue loading, one of the most widely adopted design methods, initially proposed by Neuber [16], uses the stress near the notch being designed averaged over small material units like crystals or structural particles. Nowadays, this approach is often referred to as the Line Method (LM). Using the same theoretical framework, Peterson [17] later simplified Neuber's approach by adopting as reference design stress the stress value at a specific distance from the notch tip and then comparing it to the plain fatigue limit. This approach is also known as the Point Method (PM). In both Neuber's LM and Peterson's PM, the adopted critical distance depends on the micromechanical material properties, so this length is not affected by the profile of the notch being assessed. The design approaches developed by Neuber and Peterson are well-suited for assessing notch fatigue strength in the high-cycle fatigue regime.

The Theory of Critical Distances (TCD), as proposed by Tanaka [18] and Taylor [19], represents a reformulation of Neuber and Peterson's idea based on the Linear-Elastic Fracture Mechanics (LEFM) concepts. To apply the TCD, the needed material critical length, L, is calculated from the threshold value of the stress intensity factor range, ΔK<sub>th</sub>, and the plain fatigue limit, Δσ<sub>0</sub>, according to the following formula [18–20]:

$$L = \frac{1}{\pi} \left( \frac{\Delta K_{th}}{\Delta \sigma_0} \right)^2 \quad (1)$$

It is well-known that the load ratio, R=σ<sub>min</sub>/σ<sub>max</sub>, affects the fatigue behaviour of engineering materials; hence, for a given material, L is expected to change as R varies.

In the LEFM-based TCD, the effective stress is the key design parameter that is used to estimate the high-cycle fatigue strength of materials weakened by stress concentrators of all kinds. The TCD effective stress can be calculated according to either the PM, LM, Area Method, or Volume Method. The mathematical formulations of the effective stress determined according to the PM and LM are given by Eqs. (2) and (3), respectively, with the visual interpretation of these definitions being seen in Fig. 1b:

$$\Delta \sigma_{eff} = \Delta \sigma_y \left( \theta = 0, r = \frac{L}{2} \right) \quad (2)$$

$$\Delta \sigma_{eff} = \frac{1}{2 \bullet L} \int_0^{2 \bullet L} \Delta \sigma_y(\theta = 0, r) \bullet dr \quad (3)$$

The Area Method (Fig. 1c) and Volume Method are the bi-dimensional and three-dimensional formalisation of the TCD, respectively. They involve averaging the linear-elastic stress either over a semi-circular area or over a hemisphere, with both integration domains being centred at the notch/crack tip [21]. However, since these two versions of the TCD are difficult to use in practice due to the complexities associated with the mathematical integration of the local stress over bi-dimensional/three-dimensional reference domains [22], these two formalisations of the TCD will not be considered in the present investigation.

Turning back to the determination of critical distance L, an alternative procedure for its estimation involves two distinct fatigue curves (Fig. 1d), i.e. one generated by testing plain specimens and another one by testing specimens containing notches with known profile [23,24]. Both calibration curves are to be generated under the same load ratio, R. From a mathematical point of view, these two curves can be expressed using the following classic equations:

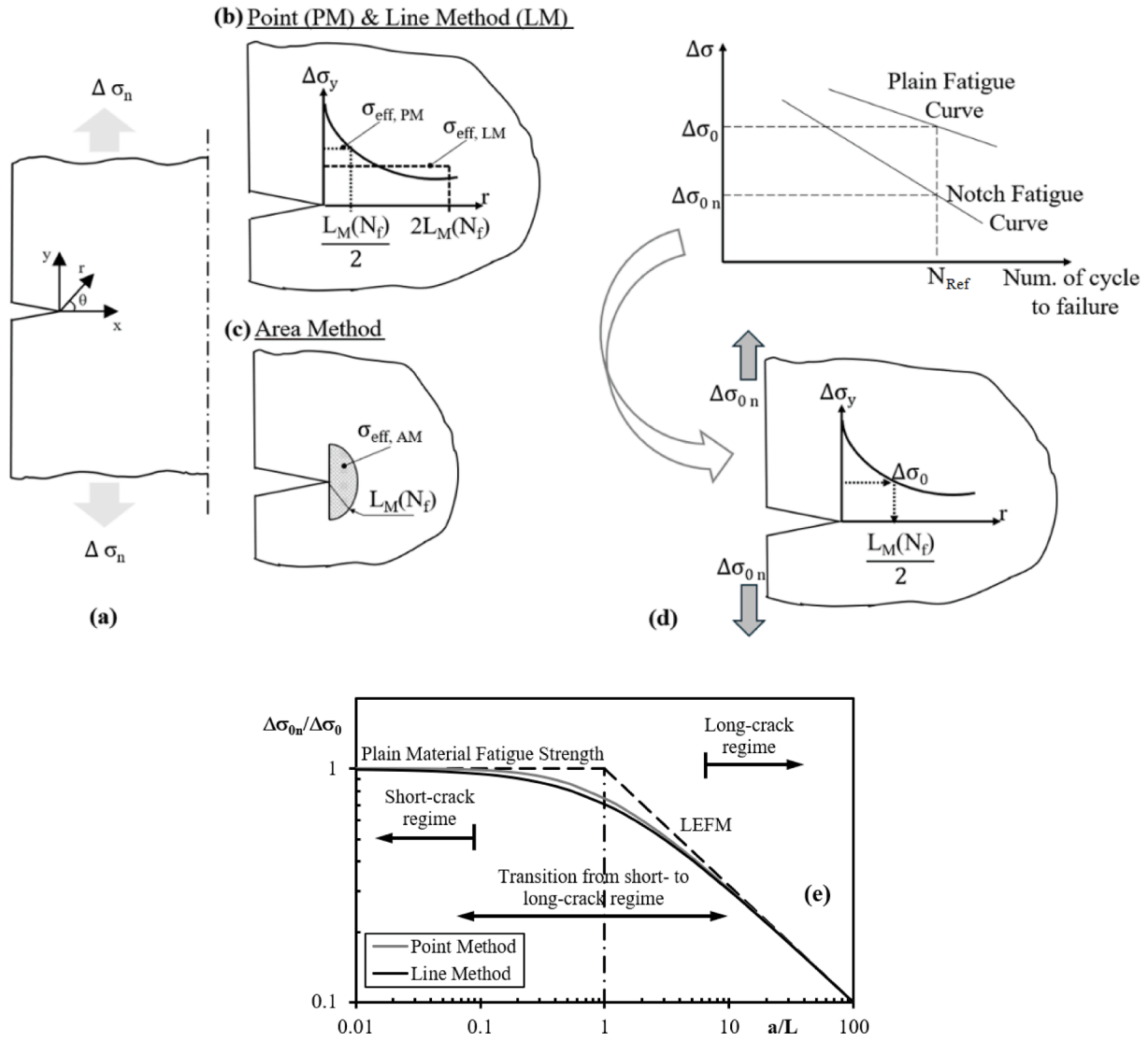


Fig. 1. Notched/cracked plate under cyclic axial loading (a); Effective stress determined according to the PM and LM (b) as well as to the Area Method; Calibration of the critical distance  $L_M$  as a function of  $N_f$  through fatigue curves from both plain and notched specimens (d); Kitagawa-Takahashi diagram and TCD (e).

$$N_f = N_{Ref} \cdot \left( \frac{\Delta\sigma_0}{\Delta\sigma} \right)^k \quad (5a)$$

$$N_f = N_{Ref} \cdot \left( \frac{\Delta\sigma_{0n}}{\Delta\sigma_n} \right)^{k_n} \quad (5b)$$

In the above relationships,  $\Delta\sigma_0$  and  $\Delta\sigma_{0n}$  are the plain and notch endurance limit range, respectively, both extrapolated at  $N_{Ref}$  cycles to failure, whereas  $k$  and  $k_n$  are the negative inverse slope of the two curves. As far as notched specimens are concerned, the nominal stress quantities used in Eq. (5b), i.e.  $\Delta\sigma_n$  and  $\Delta\sigma_{0n}$ , are calculated by referring either to the nominal net area or to the nominal gross area.

By analysing together these two calibration SN curves, critical distance  $L$  can be determined unambiguously. Consider the testing conditions resulting in the fatigue failure of both the plain and the notched material at a number of cycles to failure equal to  $N_{Ref}$ . The PM-based approach to determine  $L$  involves identifying in the notched specimen the distance,  $L/2$ , at which the range of the linear-elastic stress perpendicular to the notch bisector matches the stress range required to cause failure in the parent, plain material at  $N_f = N_{Ref}$  (Fig. 1d). This calibration process allows  $L$  to be determined by extrapolating the endurance limits to  $N_{Ref}$  cycles to failure (in the high-cycle fatigue regime). The primary advantage of this approach is its ability to estimate

$L$  accurately without the complexities associated with the elimination of the fatigue limit in real components [25]. Further, determining material fatigue constant  $\Delta K_{th}$  using standard techniques can be challenging. Firstly, it requires sophisticated equipment and skilled operators. Secondly, the process is often time-consuming and expensive. Thirdly, it can be challenging to produce specimens that perfectly match standard requirements, particularly when LEFM specimens need to be machined from real components. In this context, it is important to note that this procedure is relatively insensitive to the notch profile, provided that the critical distance is estimated using sharp notches, as outlined in references [26] and [27].

These are the reason why the validation of the approach proposed in this paper will be based on this strategy for the calculation of the critical distance.

An important feature of the TCD is that it can describe accurately the transition from the short-crack to the long-crack regime under threshold conditions [19,24]. In particular, similar to the well-known empirical equation proposed by El Hadad et al. [28], the TCD, applied in the form of the PM and LM, can gradually bridge the gap between the regions governed by LEFM and continuum mechanics principles (Fig. 1e). This enables a significant improvement in the accuracy of estimates in the transition region, where both LEFM and continuum mechanics

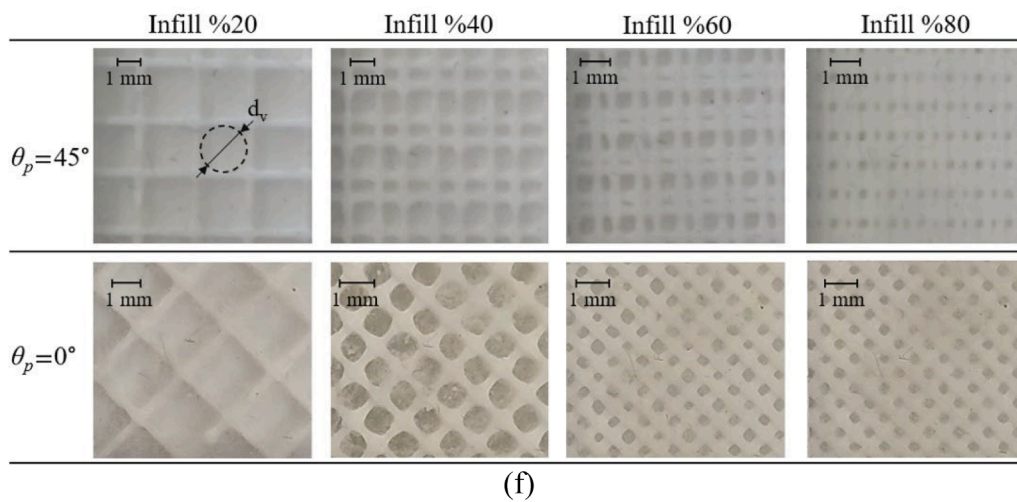
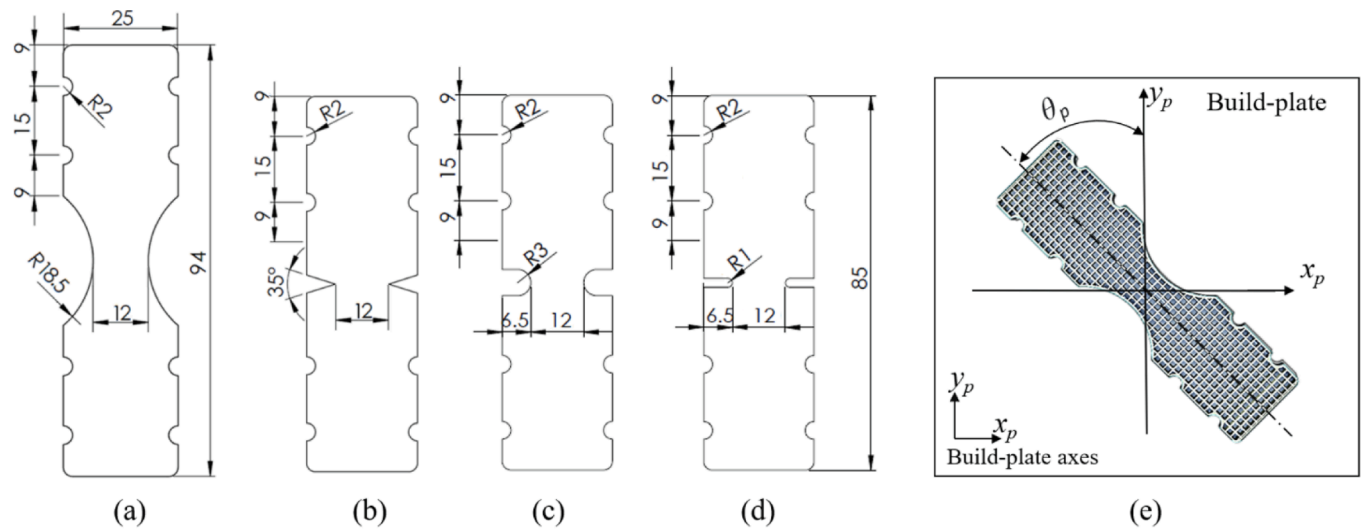


Fig. 2. Dimensions of the plain (a) and notched (b, c, and d) AM specimens of PLA being tested; Definition of raster angle  $\theta_p$  and orientation of the deposition filaments (e); fatigue testing set-up (f); AM patterns manufacture by adopting different raster angles (top to bottom), in-fill levels (left to right) and definition adopted for  $d_v$  (g).

approaches would otherwise yield non-conservative results [19]. As to this aspect, it is important to recall that, using Westergaard's classic solution for a centrally cracked infinite plate under tension [29], it is possible to write the PM and LM in explicit form to assess high-cycle fatigue strength as moving from the short-crack to the long-crack region as follows [24]:

$$\Delta\sigma_{0n} = \Delta\sigma_o \sqrt{1 - \left(\frac{a}{a + \frac{L}{2}}\right)^2} \quad (7)$$

$$\Delta\sigma_{0n} = \Delta\sigma_o \sqrt{\frac{L}{a + L}} \quad (8)$$

In Eqs (7) and (8),  $a$  is the semi-crack length and  $L$  is the TCD critical distance. In Section 4, Eqs (7) and (8) will be used to formalise an approach suitable for modelling the effect on the fatigue strength of the in-fill level in 3D-printed PLA.

Regardless of the method used for calculating  $\Delta\sigma_{\text{eff}}$ , a notched component is assumed to be at the fatigue limit when the effective stress range is less than or equal to the un-notched material fatigue (or endurance) limit,  $\Delta\sigma_o$ . Conversely, if  $\Delta\sigma_{\text{eff}}$  exceeds  $\Delta\sigma_o$ , the component is expected to fail in the medium-cycle fatigue regime. Predicting the lifetime in this regime requires adopting a difference definition for the critical distance, where this new definition explicitly accounts for the number of cycles to failure as follows [22,23]:

$$L_M(N_f) = A \cdot N_f^B \quad (9)$$

In definition (9),  $A$  and  $B$  are material constants that must be determined experimentally. Although the values of  $A$  and  $B$  for a specific material may vary with changes in the load ratio, they remain unaffected by variations in the profile or the sharpness of the geometrical feature being assessed [22,30]. For a given material and load ratio, constants  $A$  and  $B$  in Eq. (9) can be directly determined by following the procedure outlined above for the endurance limit case and illustrated in Fig. 1d. According to the PM, two calibration fatigue curves are required, i.e., the plain fatigue curve and a fatigue curve generated by testing specimens containing a known geometrical feature. The critical distance value,  $L_M/2$ , is then determined in the medium-cycle fatigue regime for two distinct values of  $N_f$ , with these  $L_M$  values being directly used to estimate the constants  $A$  and  $B$  in Eq. (9) [22,30].

Having calibrated the  $L_M$  vs.  $N_f$  power law, the TCD can be used in the form of the PM and LM by rewriting Eqs (2) and (3) as follows [22]:

$$\Delta\sigma_{\text{eff}} = \Delta\sigma_y \left( \theta = 0, r = \frac{L_M(N_f)}{2} \right) \quad (10)$$

$$\Delta\sigma_{\text{eff}} = \frac{1}{2 \cdot L_M(N_f)} \int_0^{2 \cdot L_M(N_f)} \Delta\sigma_y(\theta = 0, r) \cdot dr \quad (11)$$

By so doing, the effective stress,  $\Delta\sigma_{\text{eff}}$ , determined as above can directly be used along the plain material fatigue curve, Eq. (5a), to estimate the fatigue lifetime of the notched/cracked material under investigation. Eqs (5a), Eqs. (9)–(11) clearly demonstrates that the fatigue life of notched/cracked components can be predicted using the TCD, provided that appropriate recursive numerical methods are applied [22]. This stems from the fact that while  $N_f$  (the fatigue life) is the unknown variable in the design problem, it is also required to calculate the critical distance from Eq. (9). However, as noted in Ref. [22], this is a straightforward issue that can be resolved using standard numerical optimisation techniques.

The well-established body of knowledge briefly reviewed in this section will be used in what follows to formalise an approach suitable for performing the fatigue assessment of plain and notched PLA additively manufactured with different in-fill levels.

### 3. Details of the additively manufactured specimens, experimental setup and results

Specimens with thickness of 5 mm were used to assess the accuracy of the TCD as re-formulated in the following sections. The nominal dimensions of the plain and notched specimens being fabricated and tested are shown in the technical drawings reported in Fig. 2a to 2d. For the V-notched specimens, although the notch root radius,  $r_n$ , was set to zero in the solid model used for the AM process, the actual average root radius was measured to be 0.15 mm.

The AM specimens were all produced under the same conditions with an Ultimaker® 2 Extended+ printer. New Verbatim® white PLA filament with an initial diameter of 2.85 mm was used. The filament had density equal to 1.24 g/cm<sup>3</sup> and a glass transition temperature of 58 °C. According to its datasheet, the 0.2% offset yield strength of the parent material was equal to 63 MPa. The additive manufacturing parameters were set as follows: diameter of the brass nozzle equal to 0.4 mm, wall

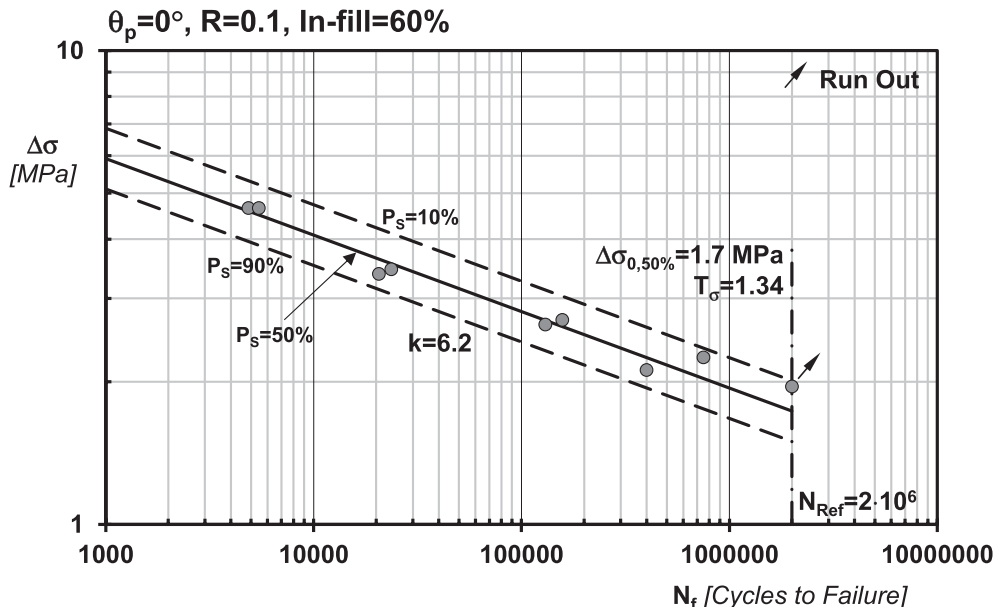


Fig. 3. S-N curve obtained by post-processing test results of a plain specimen with a raster angle  $\theta_p = 0^\circ$ , in-fill level equal to 60% and subjected to a load ratio of 0.1.

**Table 1**

Summary of the experimental results generated by testing the un-notched specimens with different infill levels.

Infill Level	$\theta_p$ [°]	R	$\Delta\sigma_{0, 50\%}$ [MPa]	k	$T_\sigma$	N. of tests	$d_v$ [mm]
100 %	0	-1	6.3	7.0	1.40	13	-
100 %	45	-1	5.5	8.0	1.50	7	-
100 %	0	0.1	3.9	8.4	1.42	12	-
80 %	0	-1	2.8	4.0	1.42	9	0.30
80 %	45	-1	3.8	6.1	1.49	9	0.26
80 %	0	0.1	2.5	7.7	1.21	9	0.30
60 %	0	-1	2.4	4.2	1.46	9	0.40
60 %	45	-1	2.7	5.3	1.47	8	0.53
60 %	0	0.1	1.7	6.2	1.34	9	0.40
40 %	0	-1	1.3	3.8	2.05	8	0.75
40 %	45	-1	2.6	8.3	1.37	8	0.84
40 %	0	0.1	0.9	4.1	1.53	11	0.75
20 %	0	-1	1.6	4.6	1.53	9	1.62
20 %	45	-1	1.8	6.1	1.65	10	1.60
20 %	0	0.1	0.8	4.5	1.58	9	1.62

thickness to 0.4 mm, shell thickness equal to 0.4 mm, layer height to 0.1 mm, and print speed to 30 mm/s. According to the specifications provided by the parent material manufacturer, the build plate temperature and extrusion temperature were set equal to 60 °C and 210 °C, respectively.

All specimens were printed flat on the build plate by setting the raster angle,  $\theta_p$ , equal to either 0° or 45°. The adopted definition for angle  $\theta_p$  is explained in Fig. 2e. Plain specimens printed at both angles were tested under a load ratio of -1, while only those printed at 0° were tested under a load ratio of 0.1. The notched specimens were manufactured with a raster angle consistently set to 0° and then tested under load ratios of -1 and 0.1. As illustrated in Fig. 2e, the Ultimaker® 2 Extended+ printer's default settings created internal voids and internal walls within the infill volume by placing the filaments at  $\pm 45^\circ$  relative to the primary printing axis, regardless of the raster angle used.

The specimens employed to run the fatigue tests were printed by exploring five different in-fill levels, i.e. 100%, 80%, 60%, 40%, and 20 %. As far as plain specimens are concerned, Fig. 2f shows the four in-fill levels lower than 100 % printed by setting the raster angle,  $\theta_p$ , equal to 0° and 45°. Fig. 2f also illustrates the definition that was adopted for the effective void size,  $d_v$  [15]. As observed in the figure,  $d_v$  varied not only as the in-fill level changed, but also among voids within the same in-fill level. Therefore, for any considered value of the in-fill level, an average  $d_v$  value was used in the calculations. In the notched specimens,  $d_v$  was determined by averaging the size of the manufacturing voids measured near the notch tip, specifically in the fatigue crack initiation region. The average values of  $d_v$  measured for the different in-fill level being considered are summarised in Tabs 1 to 4.

The AM specimens were tested under constant amplitude fatigue loading at room temperature, where high-strength bolts were used to clamp the samples in the mechanical grips (Fig. 2g). During the tests, an axial loading cell and an LVDT (Fig. 2g) were used to measure and record the instantaneous values of force and displacement. The tests were terminated if the specimen failed or after reaching  $2 \cdot 10^6$  cycles (run out).

The fracture behaviour of specimens with in-fill levels below 100 % closely resembled that of plain and notched 100% in-fill specimens [13,31]. Crack initiation consistently occurred on planes nearly perpendicular to the applied cyclic axial load, indicating a Mode I-dominated damage mechanism. Initial cracks were typically on the order of the shell thickness (approximately 0.4 mm). Subsequent crack growth progressed along zig-zag paths, following the orientation of the internal filament structure. This growth phase involved a combination of three failure mechanisms: (i) debonding between adjacent filaments, (ii) debonding between adjacent layers, and (iii) direct filament fracture.

As an example, the Wöhler diagram reported in Fig. 3 shows the

**Table 2**

Summary of the experimental results generated by testing the V-notched specimens manufactured with different in-fill levels.

Infill Level	$\theta_p$ [°]	R	$\Delta\sigma_{0n, 50\%}$ [MPa]	$k_n$	$T_\sigma$	N. of tests	$d_v$ [mm]
100 %	0	-1	2.5	3.9	1.17	8	-
100 %	0	0.1	2.2	5.6	1.64	8	-
80 %	0	-1	2.7	5.6	1.55	8	0.20
80 %	0	0.1	2.0	6.5	1.22	8	-
60 %	0	-1	1.8	4.8	1.31	8	0.39
60 %	0	0.1	1.6	5.4	1.71	9	-
40 %	0	-1	1.4	4.4	1.76	8	0.73
40 %	0	0.1	1.1	5.1	1.44	9	-
20 %	0	-1	1.5	5.4	1.59	8	1.57
20 %	0	0.1	1.5	7.6	1.33	6	-

**Table 3**

Summary of the experimental results generated by testing the U-notched specimens with notch root radius equal to 1 mm and manufactured with different in-fill levels.

Infill Level	$\theta_p$ [°]	R	$\Delta\sigma_{0n, 50\%}$ [MPa]	$k_n$	$T_\sigma$	N. of tests	$d_v$ [mm]
100 %	0	-1	3.3	4.7	1.43	7	-
100 %	0	0.1	2.6	6.8	1.27	8	-
80 %	0	-1	2.6	5.0	1.20	8	0.23
80 %	0	0.1	1.9	5.7	1.39	8	-
60 %	0	-1	1.5	3.7	1.80	10	0.38
60 %	0	0.1	1.5	5.5	1.60	8	-
40 %	0	-1	1.3	4.5	1.47	7	0.75
40 %	0	0.1	1.2	6.4	1.27	8	-
20 %	0	-1	1.2	5.7	1.28	7	1.66
20 %	0	0.1	1.0	6.4	1.14	8	-

**Table 4**

Summary of the experimental results generated by testing the U-notched specimens with notch root radius equal to 3 mm and manufactured with different in-fill levels.

Infill Level	$\theta_p$ [°]	R	$\Delta\sigma_{0n, 50\%}$ [MPa]	$k_n$	$T_\sigma$	N. of tests	$d_v$ [mm]
100 %	0	-1	4.6	5.8	1.29	10	-
100 %	0	0.1	2.8	5.4	1.53	8	-
80 %	0	-1	2.6	4.0	1.36	8	0.23
80 %	0	0.1	2.4	6.1	1.69	8	-
60 %	0	-1	2.7	7.9	1.24	8	0.42
60 %	0	0.1	1.4	4.1	1.50	9	-
40 %	0	-1	1.9	6.5	1.41	9	0.77
40 %	0	0.1	1.4	6.2	1.31	8	-
20 %	0	-1	1.6	5.8	1.19	8	1.66
20 %	0	0.1	1.0	5.2	1.63	8	-

fatigue results from plain specimens with a 60% in-fill level, produced with a raster angle,  $\theta_p$ , equal to 0° and tested under a load ratio of 0.1. The chart of Fig. 3 plots, on a log-log scale, the nominal stress range,  $\Delta\sigma$ , versus the number of cycles to failure,  $N_f$ . In the present investigation, the nominal stresses in the plain AM material were calculated by disregarding the presence of the voids. The fatigue curves seen in Fig. 3 were determined for a Probability of Survival,  $P_S$ , equal to 90%, 50%, and 10%, respectively, and were estimated, with a 95% confidence level, by assuming a log-normal distribution of the number of cycles to failure at each stress level [32]. The endurance limit for  $P_S = 50\%$  was extrapolated to  $N_{Ref} = 2 \cdot 10^6$  cycles to failure, resulting in a stress range,  $\Delta\sigma_0$ , equal to 1.7 MPa. The negative inverse slope of the curve,  $k$ , was calculated to be equal to 6.2, and the scatter ratio,  $T_\sigma$ , of the endurance limit for  $P_S = 90\%$  and  $P_S = 10\%$  to 1.34.

The above fatigue reference quantities were determined for all the testing configurations being investigated and are summarised in Table 1 for the un-notched specimens and in Tables 2 to 4 for the notched

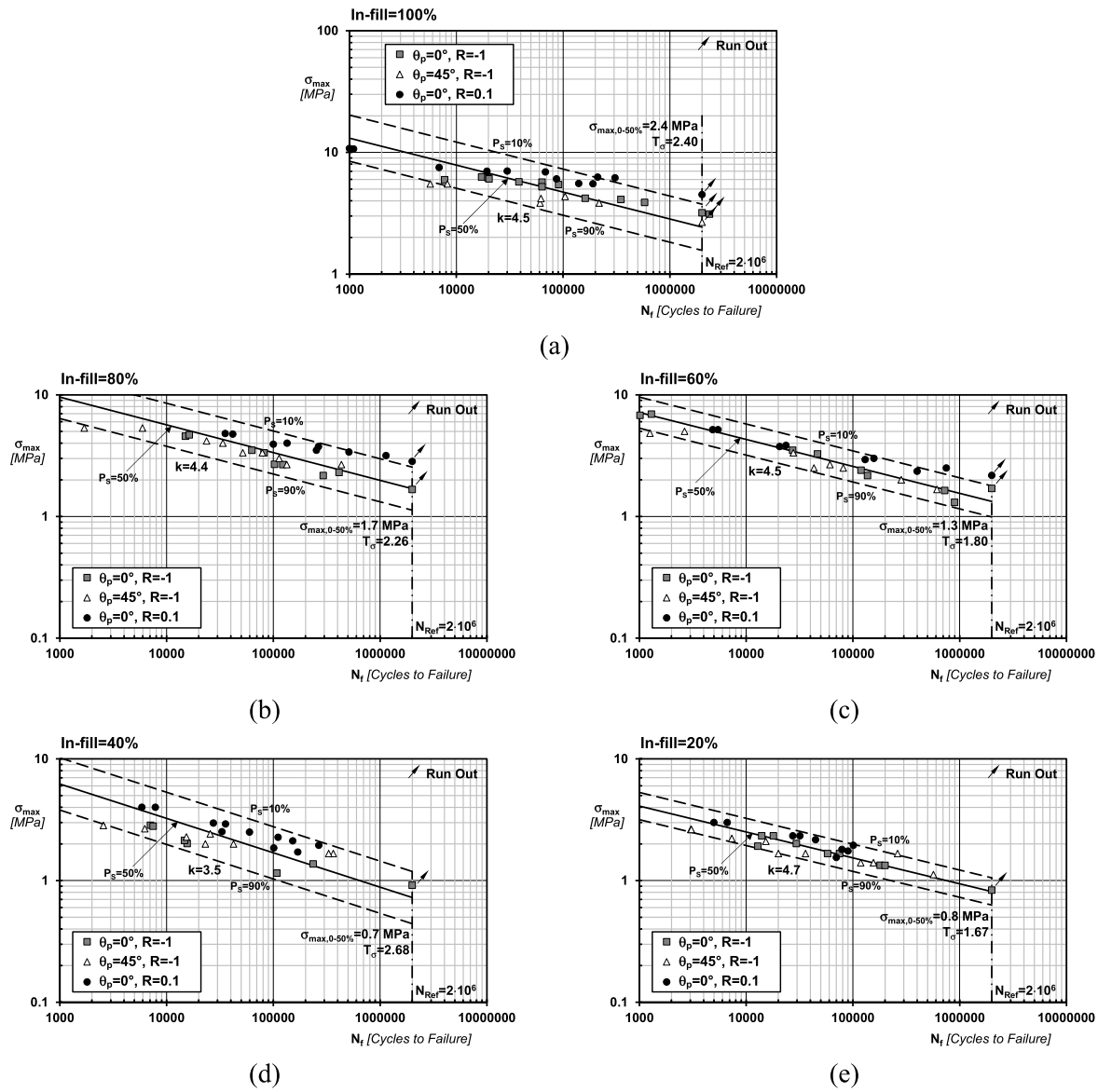


Fig. 4. Experimental results generated by testing the un-notched specimens manufactured with different in-fill levels and different raster angles under load ratios of  $-1$  and  $0.1$ .

specimens. The fatigue results generated by testing the notched specimens were post-process in terms of nominal stressed referred to the net area and calculated by disregarding the presence of the voids. As expected, [Tabs 1 to 4](#) clearly show that, for a given load ratio, raster angle and geometry, increasing the in-fill level led to a higher endurance limit. In contrast, the negative inverse slope remained unchanged at approximately 5, regardless of the in-fill level, load ratio, or specimen geometry. This value of the negative inverse slope is consistent with that reported in a previous study for an in-fill level of 100% [13].

The S-N graphs seen in [Figs. 4 to 7](#) present all the fatigue results obtained from testing both the plain and notched specimens. In constructing these graphs, the stresses for in-fill levels below 100% were calculated without accounting for the presence of the manufacturing voids. For the notched specimens, the stresses were based on the nominal net area. Additionally, as recommended in Refs [13,31], these fatigue results were analysed in terms of the maximum stress in the cycle to account for the mean stress effect on the fatigue behaviour of AM PLA in a simplified, engineering manner. The standard deviations associated with the scatter bands shown in [Figs. 4 to 7](#) were calculated (in units of the logarithm of the number of cycles to failure) as 0.48, 0.42, 0.31,

0.41, and 0.29 for infill levels of 100%, 80%, 60%, 40%, and 20%, respectively. Finally, it is worth noting that although a few run-out results were obtained, it is not possible to draw conclusions about the existence of a fatigue limit, similar to that observed in some metallic materials when tested under controlled laboratory conditions.

#### 4. Estimating fatigue lifetime of un-notched AM PLA with different in-fill levels

Building on findings from previous experimental studies [13,15,31,33], the TCD-inspired approach outlined in this section is based on the following simplifying assumptions that hold as long as PLA objects are additively manufactured flat on the build plate.

- The influence of the raster angle can be ignored, allowing AM PLA to be treated as a homogeneous and isotropic material [13,31].
- The stress-strain behaviour of AM PLA can be accurately represented using a linear-elastic constitutive model.

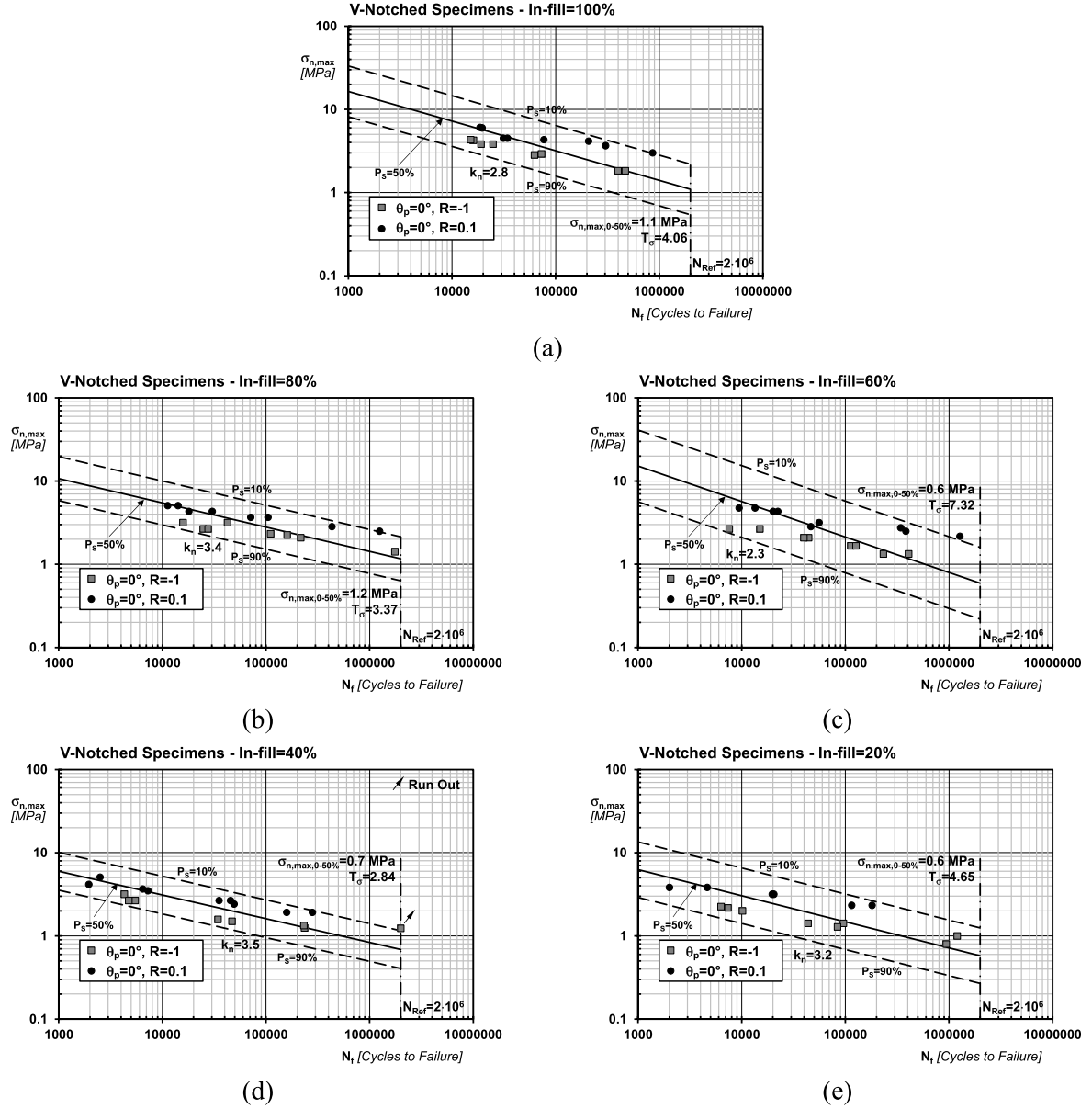


Fig. 5. Experimental results generated by testing the V-notched specimens manufactured with different in-fill levels under load ratios of  $-1$  and  $0.1$ .

- The impact of superimposed static stresses on the fatigue strength of AM PLA can be directly accounted for through the maximum stress in the cycle.

According to Table 1 and Fig. 4, the fatigue strength of plain 3D-printed PLA decreases with lower in-fill densities. Consequently, the initial step in formalising the proposed method is to establish a strategy for predicting the fatigue life of plain 3D-printed PLA components with varying internal void sizes.

Consider an un-notched strip of AM PLA as shown in Fig. 8a. The strip is 3D-printed with an in-fill density below 100 %, creating internal voids of equivalent size  $d_v$  (Fig. 8a). This strip is subjected to a cyclic axial load, with  $\sigma_{max}$  representing the maximum stress in each cycle.  $\sigma_{max}$  is assumed to be calculated by disregarding the presence of manufacturing voids. In other words, the stress analysis is conducted using fundamental solid mechanics principles, assuming the material under investigation behaves as a continuous, homogeneous solid. It is hypothesised that this strip will fail after a specific number of cycles, denoted as  $N_f$ .

Consider now an infinite plate (Fig. 8b) made of a continuous, homogeneous, isotropic, and linear-elastic material. This material has a fatigue strength identical to that determined experimentally by testing 100 % in-fill density specimens of the same AM material as the strip in Fig. 8a. The infinite plate in Fig. 8b contains a central crack extending through its thickness, with a semi-length of  $a_{eq}$ . This crack length is selected such that the plate fails after  $N_f$  cycles when the infinite plate is subjected to a remote fatigue stress with a maximum value of  $\sigma_{max}$ . Because the specimen in Fig. 8b is idealised as an infinite plate with a central through-thickness crack, its corresponding LEFM shape factor is always equal to one, regardless of the crack's semi-length,  $a_{eq}$ .

The next step in the argument is to postulate a direct relationship between the semi-length of the crack in the plate of Fig. 8b and the size of the manufacturing voids in the plain strip of Fig. 8a, i.e.:

$$a_{eq} = f(d_v) \tag{12}$$

In Eq. (12),  $f(d_v)$  acts as a transformation function, converting the AM plain strip of Fig. 8a into an equivalent continuous, homogeneous, isotropic, linear-elastic material with a central crack (Fig. 8b). The

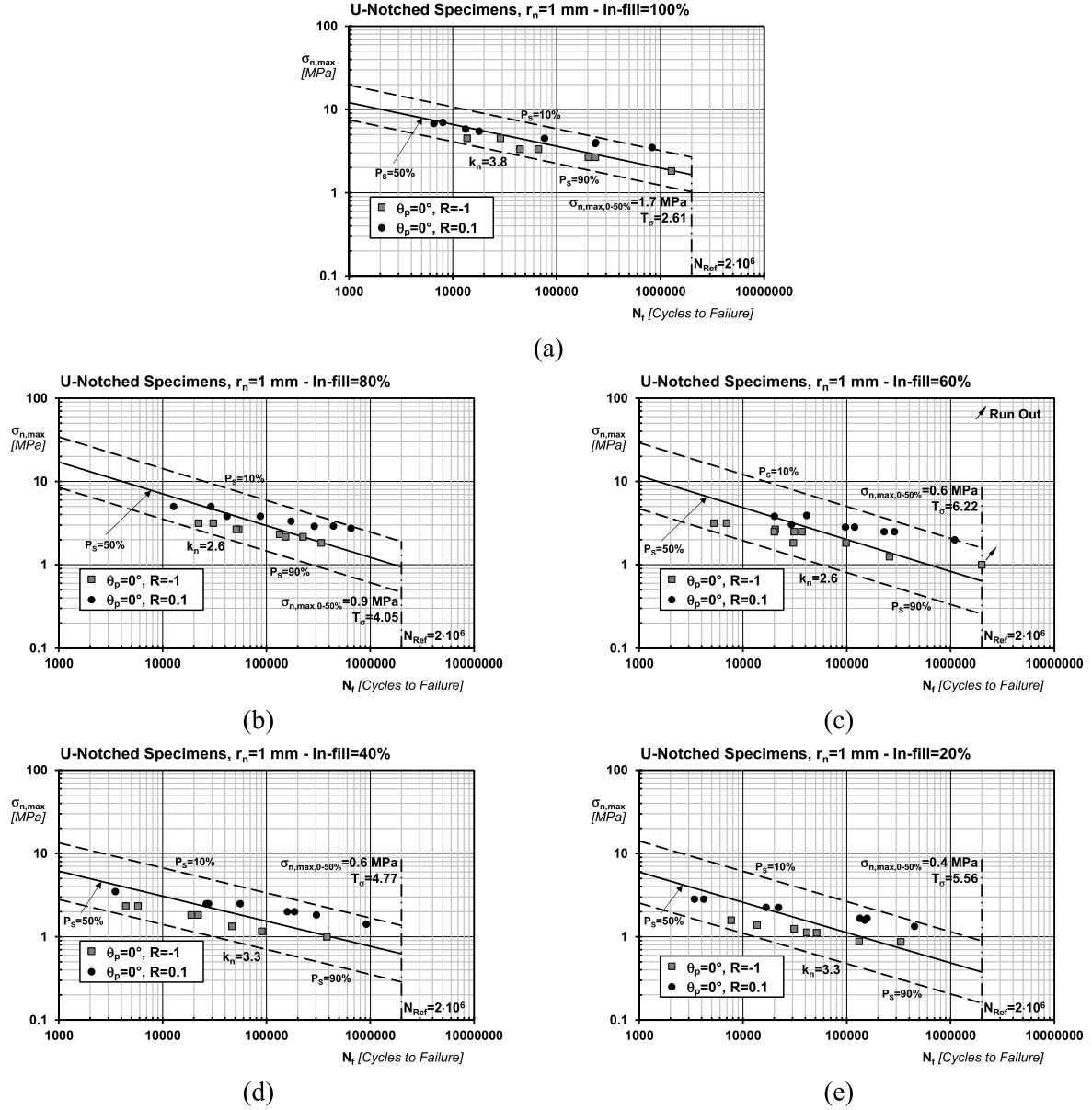


Fig. 6. Experimental results generated by testing the U-notched specimens with notch root radius equal to 1 mm and manufactured with different in-fill levels under load ratios of  $-1$  and  $0.1$ .

underlying principle of this transformation is that equivalence between the two scenarios illustrated in Fig. 8a and 8b is established by ensuring that both the AM strip and the cracked plate fail under the applied cyclic stress (having maximum value equal to  $\sigma_{max}$ ) after the same number of cycles,  $N_f$ . This approach is valid when calculating the maximum stress in the cycle,  $\sigma_{max}$ , for the AM strip by ignoring the internal voids and for the cracked plate by neglecting the presence of the crack.

Consider the TCD formulated to assess the fatigue strength of a through-thickness crack in an infinite plate under cyclic tensile loading as defined by Eqs (7) and (8). By substituting the semi-crack length,  $a$ , with the equivalent semi-crack length,  $a_{eq}$ , and using definition (9) to express the critical distance,  $L_M(N_f)$ , the PM and LM can be directly expressed as follows, respectively:

$$\sigma_{max} = \left| \sigma_{max,0} \cdot \left( \frac{N_{Ref}}{N_f} \right)^k \right|_{100\%} \sqrt{1 - \left( \frac{a_{eq}}{a_{eq} + \frac{L_M(N_f)}{2}} \right)^2} \quad (13)$$

$$\sigma_{max} = \left| \sigma_{max,0} \cdot \left( \frac{N_{Ref}}{N_f} \right)^k \right|_{100\%} \sqrt{\frac{|L_M(N_f)|_{100\%}}{a_{eq} + |L_M(N_f)|_{100\%}}} \quad (14)$$

In Eqs. (13) and (14),  $\sigma_{max,0}$  represents the endurance limit at  $N_{Ref}$  cycles to failure and  $k$  is the negative inverse slope where these two fatigue constants refer to the fatigue curve generated by testing specimens additively manufactured with 100% in-fill. Similarly,  $L_M(N_f)$  is the critical distance, Eq. (9), determined, using the procedure outlined in Fig. 1d, from calibration curves also generated by testing specimens with a 100% in-fill level. It is crucial to note that Eqs. (13) and (14) are expressed in terms of maximum stress in the fatigue cycle. This is because, as experimentally demonstrated in Refs [13,31], the maximum stress effectively accounts (from an engineering standpoint) for the mean stress effect in fatigue of AM PLA. In contrast, classic approaches such as Goodman's equation are unable to accurately account for the detrimental effect of superimposed static stresses, as highlighted in reference [31].

The final step in the argument is to define transformation function  $f$

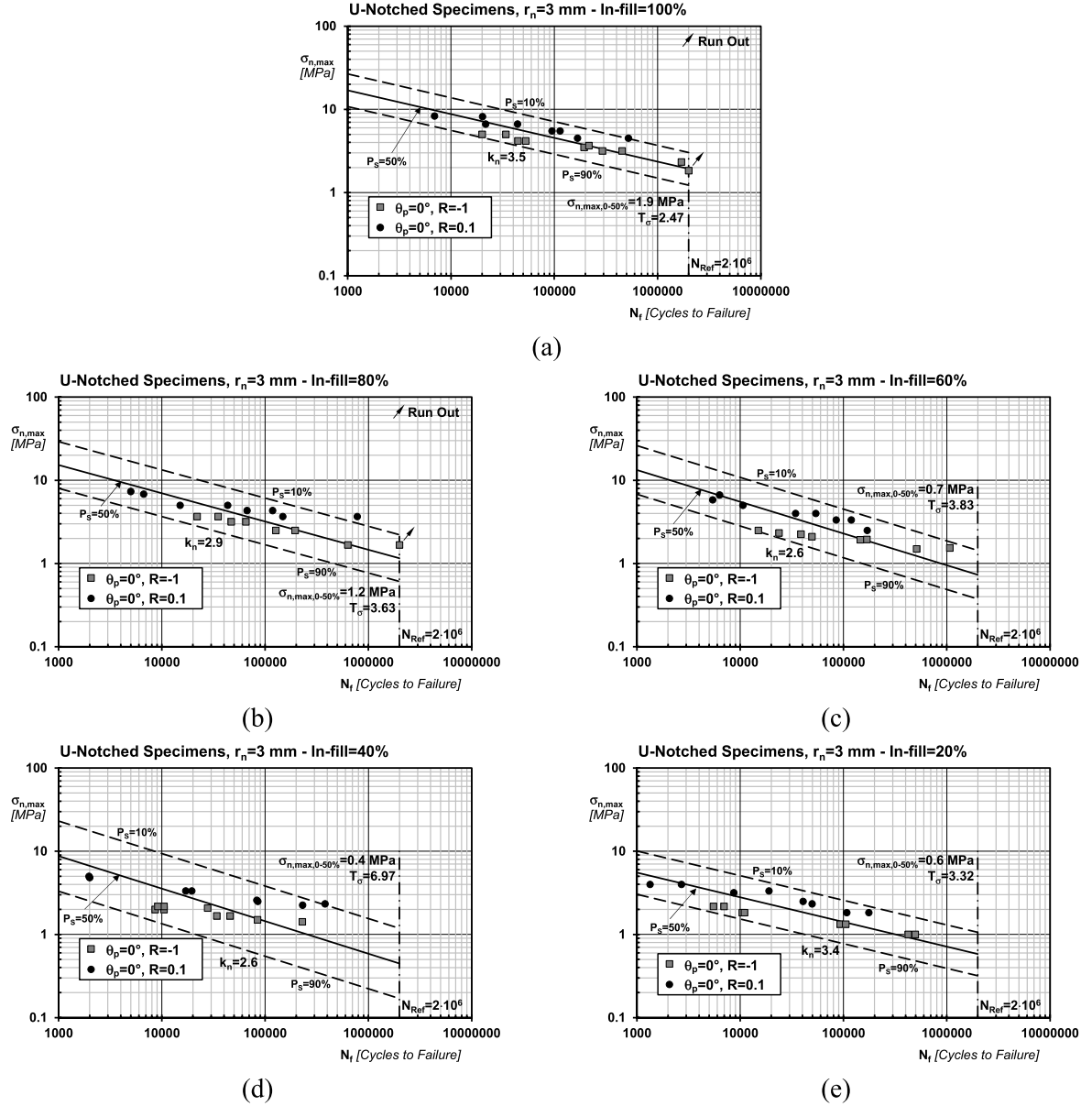


Fig. 7. Experimental results generated by testing the U-notched specimens with notch root radius equal to 3 mm and manufactured with different in-fill levels under load ratios of  $-1$  and  $0.1$ .

( $d_V$ ) and calibrate it appropriately. Ideally, this process should be optimized to minimize the experimental effort required for calibrating  $f(d_V)$ . To achieve this, as done under static loading [15], we can hypothesise that the relationship between  $a_{eq}$  and  $d_V$  is a simple linear one, expressed as follows:

$$a_{eq} = k_t \cdot d_V \quad (15)$$

where  $k_t$  is a dimensionless transformation constant that can be directly determined through experiments conducted on specimens with an in-fill level lower than 100%. Once constant  $k_t$  is calibrated in Eq. (15), the PM and LM can be directly applied to estimate the fatigue life of the AM PLA component under investigation for any in-fill level. This is achieved by simply rewriting Eqs. (13) and (14) as follows:

$$\sigma_{max} = \left| \sigma_{max,0} \cdot \left( \frac{N_{Ref}}{N_f} \right)^k \right|_{100\%} \sqrt{1 - \left( \frac{k_t \cdot d_V}{k_t \cdot d_V + \frac{A \cdot N_f^B}{2}} \right)^2} \quad (16)$$

$$\sigma_{max} = \left| \sigma_{max,0} \cdot \left( \frac{N_{Ref}}{N_f} \right)^k \right|_{100\%} \sqrt{\frac{|A \cdot N_f^B|_{100\%}}{k_t \cdot d_V + |A \cdot N_f^B|_{100\%}}} \quad (17)$$

In Eqs (16) and (17),  $\sigma_{max}$  is the maximum stress in the fatigue cycle applied to the un-notched AM component being designed (Fig. 8a). The stress analysis is conducted assuming the material is linear-elastic, continuous, homogeneous, and isotropic (i.e., by neglecting the presence of manufacturing voids). Fatigue constants  $\sigma_{max,0}$  (at  $N_{Ref}$  cycles to failure),  $k$ ,  $A$ , and  $B$  are all determined by testing specimens manufactured by setting the in-fill level equal to 100%. Consequently, fatigue life

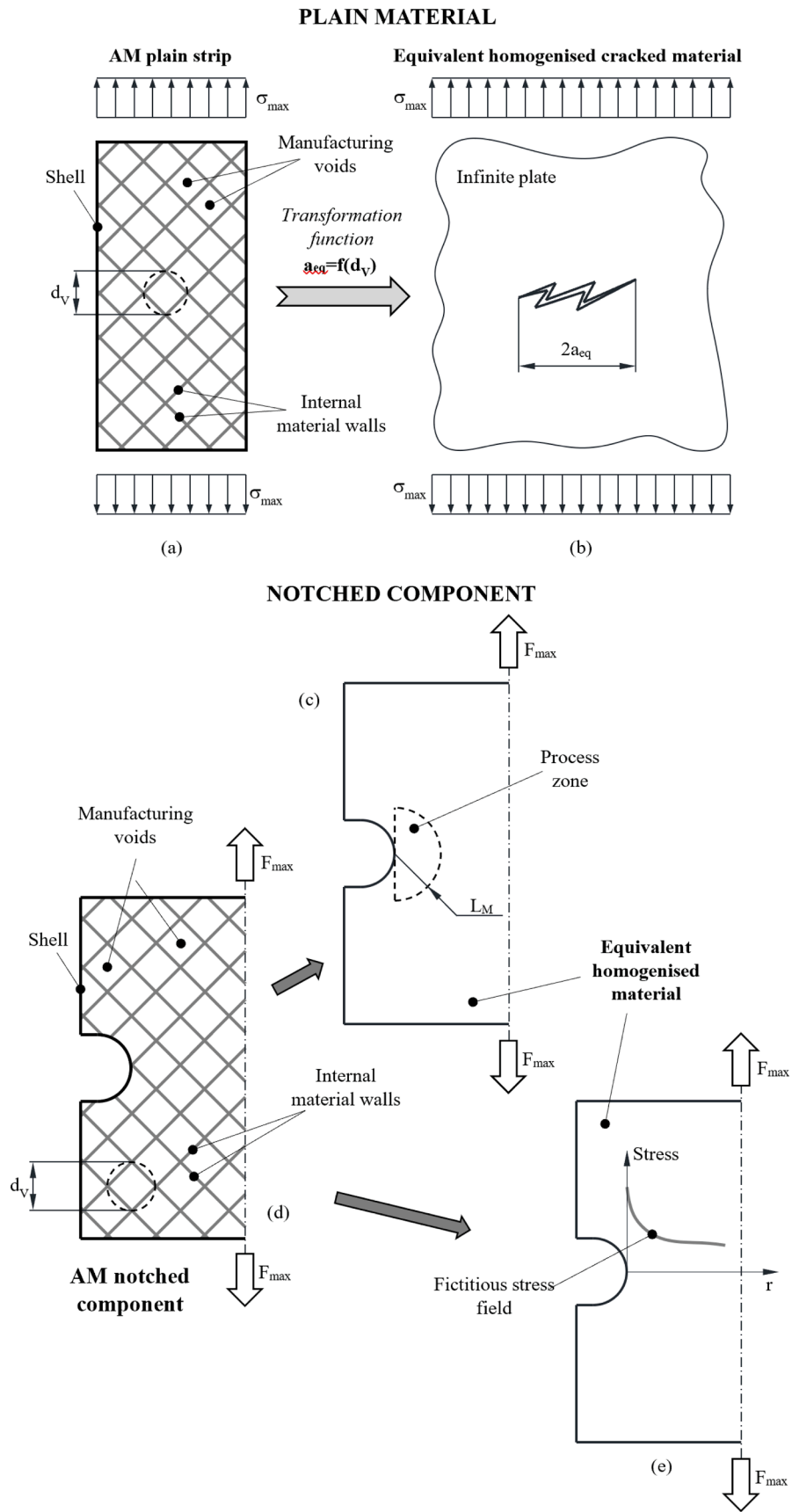


**Fig. 8.** Illustration of the transformation from a plain material with uniformly distributed manufacturing voids (a) to an equivalent homogenized cracked continuum material (b); process zone (c) and fictitious linear-elastic local stress fields (e) to estimate fatigue lifetime of notched components (d) of AM PLA.

can be calculated using the PM and LM by solving Eqs. (16) and (17) for  $N_f$ , respectively. The number of cycles to failure can be readily determined by solving the equations above using standard numerical methods.

It is worth noting that, although other cracked material configurations could be used to formalise the transformation process discussed earlier, the simplicity of a central crack in an infinite plate offers notable advantages. Specifically, the LEFM shape factor becomes irrelevant in this case, as it is invariably equal to one for a central crack in an infinite plate. This streamlines the analysis and reduces computational complexity.

Lastly, it is important to emphasise that the method developed in this section is based on a straightforward linear transformation law – see Eq. (15). However, alternative functions could be used to express  $f(d_v)$ , allowing this theoretical framework to be extended for the fatigue assessment of other materials with structural voids, such as, for instance, honeycomb structures, beyond just 3D-printed materials.

## 5. Estimating fatigue lifetime of notched AM PLA with different in-fill levels

AM excels at producing intricate geometries with precision, but this complexity can lead to localised stress concentrations that compromise structural integrity. To address this challenge, we propose and formalise in this section a combined approach using the TCD and the equivalent homogenised material concept. This framework enables accurate fatigue assessment of notched AM PLA components by providing simple yet reliable design rule.

A notched component is additively manufactured with a reduced in-fill percentage. This results in internal voids with an average size of  $d_v$ , as illustrated in Fig. 8d. This notched component is subjected to a uniaxial fatigue loading and the maximum value of the cyclic force being applied is denoted as  $F_{max}$  (Fig. 8d).

To accurately estimate fatigue strength using the TCD, we model the notched AM component seen in Fig. 8e as a continuum, homogeneous, isotropic, and linear-elastic body with identical dimensions to the component in Fig. 8d. This allows us to apply the PM and LM while assuming that the process zone remains constant, regardless of manufacturing void size (Fig. 8c). Based on this assumption, we propose that the critical distance,  $L_M$ , is determined directly using Eq. (9), with constants A and B obtained from experimental results generated by testing 100% in-fill plain specimens. As critical distance  $L_M$  remains constant for a given AM material, the detrimental effect of manufacturing voids is directly taken into account by adjusting the

material's intrinsic static strength according to either Eq. (16) or Eq. (17).

Given our assumptions of a continuum, homogeneous, isotropic, and linear-elastic AM component, the fictitious local stress fields (Fig. 8e) used for the calculation of the TCD effective stress can be determined directly through conventional FE analysis or existing analytical solutions.

Once the fictitious local stress fields are determined, the effective stress,  $\sigma_{eff,max}$ , can be calculated using the TCD in the form of either the PM, Eq. (10), or the LM, Eq. (11). Considering the weakening effect of manufacturing voids on the AM material, the failure condition at a number of cycles to failure equal to  $N_f$  can be expressed as follows:

$$\sigma_{eff,max}(N_f) = \sigma_{max}(N_f) \quad (18)$$

where the plain material fatigue strength at  $N_f$  cycles to failure,  $\sigma_{max}(N_f)$ , is determined via either Eq. (16) or Eq. (17). Note that both sides of Eq. (18) are expressed in terms of maximum stress in the fatigue cycle to incorporate the mean stress effect, as recommended in Refs [13,31]. For the PM, combining Eq. (10) and Eq. (16) allows failure condition (18) to be directly rewritten as:

$$\begin{aligned} \sigma_{y,max} \left( \theta = 0, r = \frac{A \cdot N_f^B}{2} \right) \\ = \left| \sigma_{max,0} \cdot \left( \frac{N_{Ref}}{N_f} \right)^k \right|_{100\%} \sqrt{1 - \left( \frac{k_t \cdot d_v}{k_t \cdot d_v + \frac{A \cdot N_f^B}{2}} \right)^2} \end{aligned} \quad (19)$$

Similarly, combining Eq. (11) and Eq. (17) allows failure condition (18) to be expressed according to the LM as follows:

$$\begin{aligned} \frac{1}{2 \cdot \left| A \cdot N_f^B \right|_{100\%}} \int_0^{2 \cdot \left| A \cdot N_f^B \right|_{100\%}} \sigma_{y,max}(\theta = 0, r) \cdot dr \\ = \left| \sigma_{max,0} \cdot \left( \frac{N_{Ref}}{N_f} \right)^k \right|_{100\%} \sqrt{\frac{\left| A \cdot N_f^B \right|_{100\%}}{k_t \cdot d_v + \left| A \cdot N_f^B \right|_{100\%}}} \end{aligned} \quad (20)$$

In Eqs. (19) and (20), the unknown variable is the number of cycles to failure, which appears on both sides of the equations themselves. Fatigue life can be determined using standard numerical iterative methods that combine the linear elastic fictitious stress field distribution

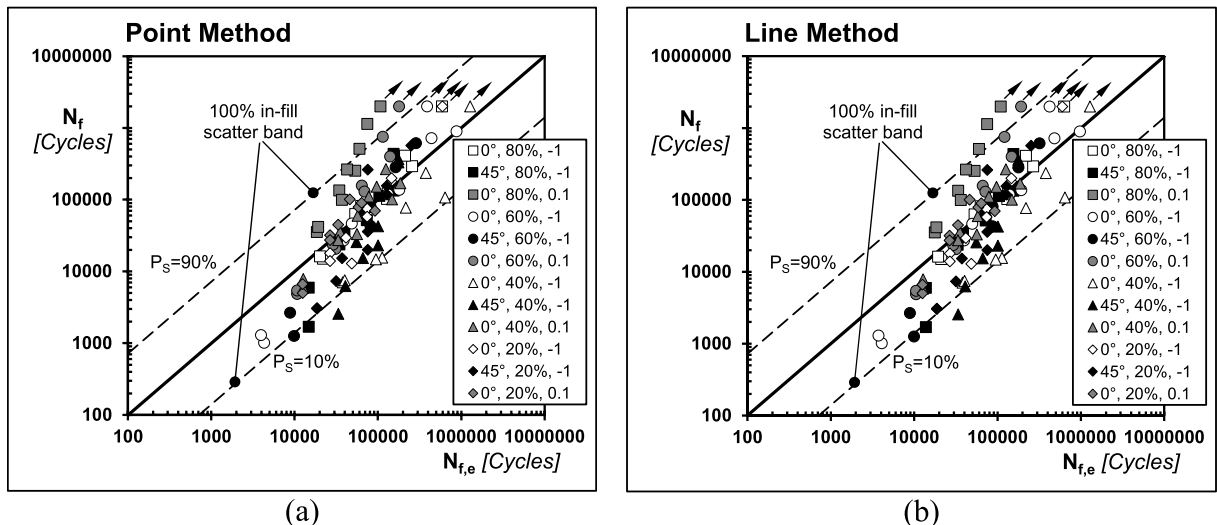


Fig. 9. Accuracy of the PM (a) and LM (b) in estimating the fatigue lifetime of the plain specimens additively manufacture with different in-fill levels.

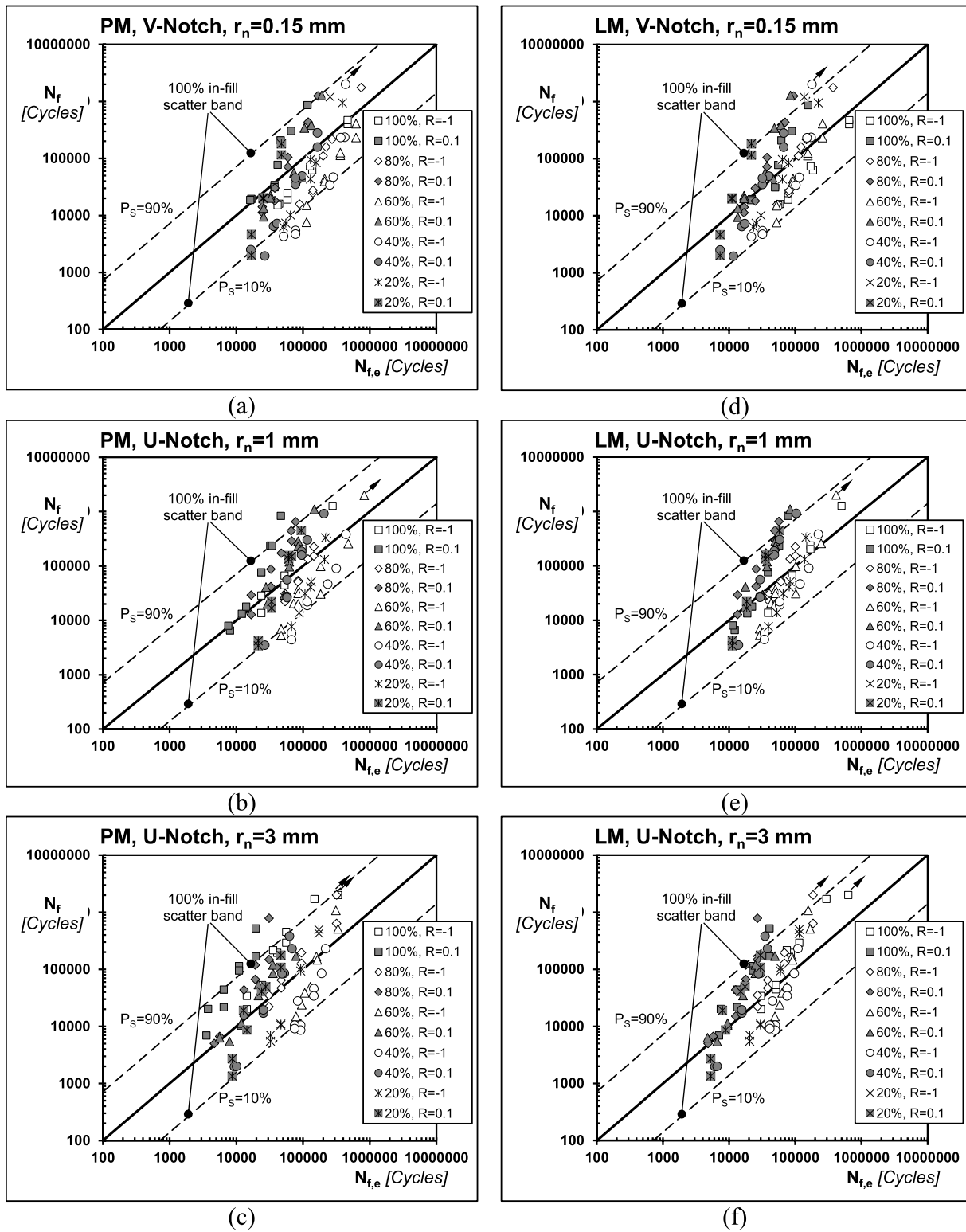


Fig. 10. Accuracy of the PM (a, b, c) and LM (d, e, f) in estimating the fatigue lifetime of the notched specimens additively manufacture with different in-fill levels.

with the PM and LM as expressed in Eqs. (19) and (20), respectively.

6. Validation by experimental results

To apply the TCD to post-process the generated fatigue results, local stresses were calculated using commercial Finite Element (FE) software ANSYS®. The relevant linear-elastic stress fields in the notched

specimens were determined by solving two-dimensional FE models constructed using 4-node structural plane elements (plane 182). In accordance with the hypotheses formed to develop the proposed approach, the numerical solutions were calculated assuming the AM polymer under investigation behaved as a linear-elastic, homogeneous, and isotropic material. This means that the voids were not modelled explicitly. To ensure adequate numerical accuracy, the mesh density

near the notch tip was gradually increased until convergence was achieved. While the solid model of the V-notched specimens for the AM process had a zero root radius, the FE analyses were conducted with a root radius of 0.15 mm, matching the average value measured from the actual manufactured specimens.

To verify the accuracy and reliability of the PM and LM, initially Eqs. (16) and (17) were used to estimate the fatigue strength of the tested un-notched specimens (see Table 1 and Fig. 4). The fatigue curves generated by testing plain (Fig. 2a) and V-notched specimens (Fig. 2b) manufactured with 100% in-fill were employed to estimate constants A and B in the  $L_M$  vs.  $N_f$  power law, Eq. (9). The procedure illustrated in Fig. 1d returned the following values for constants A and B:

$$L_M(N_f) = 25.1 \cdot N_f^{-0.242} [mm] \quad (21)$$

Subsequently, the experimental results under  $R = -1$  from plain PLA specimens additively manufactured with 80% in-fill and  $\theta_p = 0^\circ$  (Table 1) were used to calibrate transformation function  $f(d_v)$ , Eq. (15). In particular, for each calibration data point, assuming  $N_f$  was known from the experiment, the transformation constant,  $k_t$ , was calculated using both the PM and LM formulated according to Eqs. (16) and (17), respectively. The eight resulting values for the transformation constant were then averaged, yielding a  $k_t$  value of 9.4 for the PM and 8.2 for the LM.

The experimental fatigue life,  $N_f$ , vs. the estimated fatigue life,  $N_{f,e}$ , charts in Fig. 9a and b summarise the accuracy of the PM and LM, respectively, in predicting the experimental results generated by testing the un-notched specimens manufactured with different in-fill levels and raster angles. These charts clearly demonstrate that Eqs. (16) and (17) are highly accurate, with predictions from both the PM and LM predominantly falling within the scatter band of the un-notched 100% in-fill curve used for calibration. Additionally, the graphs indicate that the level of scatter for in-fill levels other than 80 % was comparable to that observed when the method was re-applied to the calibration data themselves. This further confirms the accuracy and consistency (in terms of scattering) of the approach in estimating the fatigue life of AM PLA manufactured with less than 100% in-fill.

The charts in Fig. 10 compare the experimental fatigue life,  $N_f$ , to the estimated fatigue life,  $N_{f,e}$ , for notched specimens with varying in-fill levels, highlighting the accuracy of the PM and LM. The results show that both methods, as applied in Eqs (19) and (20), accurately predicted fatigue life, with most predictions falling within the scatter band of the un-notched 100% in-fill calibration scatter band. The high accuracy of the proposed TCD-based approach is noteworthy, particularly considering its ability to design real notched AM components by post-processing standard FE results. The FE analysis can be conducted using a homogeneous, isotropic, linear-elastic material model, eliminating the need to explicitly model manufacturing voids.

## 7. Conclusion

This study experimentally and computationally investigates the influence of in-fill level on the fatigue behaviour of plain and notched AM PLA. A novel methodology, based on the TCD, is presented to predict the fatigue strength of plain and notched PLA AM components with uniformly distributed voids. Specimens were printed flat on the build plate and tested under two different load ratios. The following conclusions are drawn from the experimental and theoretical findings.

- For in-fill levels below 100% as well, the mean stress effect on the fatigue behaviour of AM PLA can be effectively accounted for during the design process by considering the maximum stress in the cycle.
- The proposed TCD-based approach, which employs an equivalent homogenised material concept, effectively correlates void size with the fatigue strength of plain AM PLA.

- The TCD-based approach being proposed is shown to be highly accurate in predicting fatigue lifetime of notched PLA additively manufactured with different in-fill levels.
- The proposed TCD-based fatigue design method can be applied by post-processing standard linear-elastic FE results, where the numerical solutions are obtained from homogeneous, isotropic models. This approach eliminates the need for explicitly modelling manufacturing voids.
- More work is needed to assess the accuracy and reliability of the proposed approach considering not only different internal manufacturing patterns, but also different materials.

## CRedit authorship contribution statement

**Mehmet F. Yaren:** Writing – original draft, Visualization, Formal analysis, Data curation. **Luca Susmel:** Writing – review & editing, Writing – original draft, Visualization, Methodology, Investigation, Funding acquisition, Conceptualization.

## Declaration of competing interest

The authors declare that they have no known competing financial interests or personal relationships that could have appeared to influence the work reported in this paper.

## Data availability

Data will be made available on request.

## References

- [1] Kirchheim A, Katrodiya Y, Zumofen L, Ehrig F, Wick C. Dynamic conformal cooling improves injection molding: hybrid molds manufactured by laser powder bed fusion. *Int J Adv Manuf Tech* 2021;114:107–16.
- [2] Bas J, Dutta T, Llamas Garro I, Velázquez-González JS, Dubey R, Mishra SK. Embedded sensors with 3D printing technology. *Sensors* 2024;24(6):1955.
- [3] Kahraman MF, Genel K. Bending performance of the AuxOcta multi-cellular beam structure. *Eng Struct* 2023;294:116737.
- [4] Khalaj R, Tabriz AG, Okereke MI, Douroumis D. 3D printing advances in the development of stents. *Int J Pharm* 2021;609:121153.
- [5] Bai L, et al. Additive manufacturing of customized metallic orthopedic implants: Materials, structures, and surface modifications. *Metals* 2019;9(9):1004.
- [6] Zhou X, Zhou G, Junka R, Chang N, Anwar A, Wang H, et al. Fabrication of poly(lactic acid) (PLA)-based porous scaffold through the combination of traditional bio-fabrication and 3D printing technology for bone regeneration. *Colloids Surf B Biointerfaces* 2021;197:111420.
- [7] Bakhtiari H, Nouri A, Tolouei-Rad M. Impact of 3D printing parameters on static and fatigue properties of poly(lactic acid) (PLA) bone scaffolds. *Int J Fatigue* 2024; 186:108420.
- [8] Jimenez-Martinez M, Varela-Soriano J, Carreón JJR, Torres-Cedillo SG. Mechanical fatigue of PLA in additive manufacturing. *Eng Fail Anal* 2023;149:107273.
- [9] Andrzejewska A, Pejkowski Ł, Topoliński T. Tensile and fatigue behavior of additive manufactured polylactide. *3D Print. Addit Manuf* 2019;6(5):272–80.
- [10] Hassanifard S, Hashemi SM. On the strain-life fatigue parameters of additive manufactured plastic materials through fused filament fabrication process. *Addit Manuf* 2020;32:100973.
- [11] Gomez-Gras G, Jerez-Mesa R, Travieso-Rodriguez JA, Lluma-Fuentes J. Fatigue performance of fused filament fabrication PLA specimens. *Mater Des* 2018;140: 278–85.
- [12] Hanon MM, Zsidai L, Ma Q. Accuracy investigation of 3D printed PLA with various process parameters and different colors. *Mater Today Proc* 2021;42:3089–96.
- [13] Ezeh OH, Susmel L. On the notch fatigue strength of additively manufactured polylactide (PLA). *Int J Fatigue* 2020;136:105583.
- [14] Algarni M. Fatigue behavior of PLA material and the effects of mean stress and notch: experiments and modeling. *Procedia Struct Integr* 2022;37:676–83.
- [15] Ahmed AA, Susmel L. Static assessment of plain/notched polylactide (PLA) 3D-printed with different in-fill levels: equivalent homogenised material concept and Theory of Critical Distances. *Fatigue Fract Eng Mater Struct* 2019;42(4):883–904.
- [16] Neuber H. *Theory of notch stresses: principles for exact calculation of strength with reference to structural form and material*. II Ed. Berlin: Springer Verlag; 1958.
- [17] Peterson RE. *Notch Sensitivity*. In: Sines G., Waisman J. L., Editors. *Metal Fatigue*. New York. McGraw Hill 1959;293-306.
- [18] Tanaka K. Engineering formulae for fatigue strength reduction due to crack-like notches. *Int J Fracture* 1983;22:R39–45.
- [19] Taylor D. Geometrical effects in fatigue: a unifying theoretical model. *Int J Fatigue* 1999;21:413–20.

- [20] El Haddad MH, Topper TH, Smith KN. Fatigue crack propagation of short cracks. *J Engng Mater Tech (ASME Trans)* 1979;101:42–5.
- [21] Bellett D, Taylor D, Marco S, Mazzeo E, Guillois J, Pircher T. The fatigue behaviour of three-dimensional stress concentrations. *Int J Fatigue* 2005;27(3):207–21.
- [22] Susmel L, Taylor D. A novel formulation of the theory of critical distances to estimate lifetime of notched components in the medium-cycle fatigue regime. *Fatigue Fract Eng Mater Struct* 2007;30(7):567–81.
- [23] Susmel L. *Multiaxial notch fatigue: from nominal to local stress–strain quantities*. Cambridge (UK): Woodhead & CRC; 2009.
- [24] Taylor D. *The Theory of Critical Distances: A New Perspective in Fracture Mechanics*. Elsevier Science; 2007.
- [25] Miller KJ, O'Donnell WJ. The fatigue limit and its elimination. *Fatigue Fract Eng Mater Struct* 1999;22:545–57.
- [26] Susmel L, Taylor D. The Theory of Critical Distances as an alternative experimental strategy for the determination of  $K_{Ic}$  and  $\Delta K_{th}$ . *Eng Fract Mech* 2010;77(9): 1492–501.
- [27] Lobato da Silva B, Ferreira JLA, Aratijo JA. Influence of notch geometry on the estimation of the stress intensity factor threshold by considering the Theory of Critical Distances. *Int J Fatigue* 2012;42:258–70.
- [28] ElHaddad MH, Dowling NF, Topper TH, Smith KN. J-integral applications for short fatigue cracks at notches. *Int J Fract* 1980;16:15–24.
- [29] Westergaard HM. Bearing pressures and cracks. *J Appl Mech A* 1939;61:49–53.
- [30] Susmel L, Taylor D. The Theory of Critical Distances to estimate lifetime of notched components subjected to variable amplitude uniaxial fatigue loading. *Int J Fatigue* 2011;33:900–11.
- [31] Ezech OH, Susmel L. Fatigue strength of additively manufactured polylactide (PLA): effect of raster angle and non-zero mean stresses. *Int J Fatigue* 2019;126:319–26.
- [32] Kufoin E, Susmel L. Quantitative review of probabilistic approaches to fatigue design in the medium cycle fatigue regime. *Probabilistic Eng Mech* 2024;75: 103589.
- [33] Ahmed AA, Susmel L. A material length scale based methodology to assess static strength of notched additively manufactured polylactide (PLA). *Fatigue Fract Eng Mater Struct* 2018;41(10):2071–98.